
# DESIGN OF LINEAR-PHASE FILTER BANKS WITH MULTIPLIER-LESS LATTICE STRUCTURES

Li Chen*, Xiyan Wang, Ronghua Peng, Fu Yang
Department of Electronic and Information Engineering,
Shantou University, Shantou 515063,
Guangdong, P. R. China

Emails: lchen@stu.edu.cn

***Submitted: July 1, 2013*** ***Accepted: Nov. 23, 2013*** ***Published: Dec. 23, 2013***

*Abstract*- **In this paper, a new multiplier-less algorithm is proposed for the design of perfect-reconstruction linear-phase (PR LP) filter banks by using multiplier-less lattice structures. The coefficients in the multiplication operations have been replaced with limited number of additions and the computational complexity is reduced significantly. The property of perfection reconstruction, however, is preserved regardless the multiplier-less approximation of lattice structures in the factorization of polyphase matrix. The coefficients in the 2x2 rotation matrices of the lattice structures are expressed as sum-of-powers-of-two (SOPOT) coefficients in the parameterization processes. By using the multiplier-less rotation matrices, the unitary matrices are constructed for the lattice factorization of perfect-reconstruction linear-phase filter banks. Design**

**examples of 5-channel and 8-channel multiplier-less linear-phase filter banks are included to validate the algorithm and implementation.**

**Index terms*:* Non-multiplier realization, perfect reconstruction, linear phase, filter bank, lattice realization, SOPOT coefficient, lattice structure.**

## I. INTRODUCTION

The design and implementation of linear-phase filter banks have received increasing attentions recently [1-21]. With wired and wireless sensor networks, multirate filter banks can be extended to a wide range of applications. Near perfect reconstruction filter banks were investigated in harmonic analysis of electrical waveforms in power systems [1][2]. Compared with the conventional filters, the filter banks have better selectivity properties which make them suitable for harmonic analysis. In [3], filter banks with data prefiltering were developed to forecast the loads in a moving window manner. Numerical testing demonstrated accurate predictions with small standard deviations for very short-term load forecasting (VSTLF). Filter banks were applied to determine vehicle velocity, the distance between axles, and the axle load in [4]. In data compression and signal enhancement in intelligent sensor networks, filter banks were also employed [5]-[11]. Filter banks have also been used in the areas of speech and image processing. In speech processing applications, computationally efficient digital FIR filter bank with adjustable subband distribution was proposed for hearing-aid applications in [12]-[14] and an oversampled filter bank with critical-band division and low delay was applied to a two-state modeling speech enhancement system in [15]. In image processing applications, a novel continuously-valued MRF model with separable filter banks and its discriminative training method were proposed for image denoising and image demosaicing in [16]. Lattice structures of biorthogonal filter banks were optimized using the SPIHT algorithm in [17] and utilized for image compressing in [17]-[18]. In [19], filter banks were proposed to diagnose broken bars and mixed eccentricity faults of an induction motor (IM) by detecting the electrical current during a startup transient. In [20], multi-stream sampling and reconstructing band-limited signals from their non-uniform recurrent samples were adopted to implement the modulation technique for three phase, voltage source, six-pulse, and ac–dc converters.

In the past years, the multiplier-less implementation has been an active research area in signal processing and circuit systems. A design of maximally flat cascaded integrator comb compensation filters was introduced in [22]. Second- and fourth-order linear phase filters were considered for narrow-band and wideband compensation. Closed-form equations for the computation of the filter coefficients were given and the multiplierless implementation was shown. In [23], a new algorithm to design FIR filters with as low adder cost as possible was presented. In contrast to the previous algorithms for either coefficient generation or multiplier-block synthesis, the proposed algorithm combined the two steps in an interleaved manner to consider the effects of the multiplier-block synthesis in optimizing the next coefficient. In [24], an implementation of a mix-radix SDF pipeline FFT processor was presented. The new multiplier-less butterfly structure was proposed using simple shift and addition/subtraction operations. In order to improve the performance, the complex multipliers were replaced by simpler and faster units which use only shift and addition/subtraction operations. In [25], a multiple real constant multiplication (MRCM) problem was formulated and investigated. In [26], a new approach was introduced to design low complexity multiplierless digital filters. Unlike traditional methods with fixed filter structures, the structures were simultaneously designed and optimized in a dynamic fashion. A class of 2-channel quadrature mirror filters was investigated in [27] and the design of filter banks with sharp transition band was reported in [28][29]. In [30], the design of multiplier-less decimation filters based on an extended search of cyclotomic polynomials (CP) was proposed. The z-transfer functions of CPs with indexes can be from 61 to 104 and from 105 to 200.

In this paper, a new multiplier-less realization of the perfect reconstruction linear-phase filter banks (PR LP FB) is presented by extending the multiplier-less approach to the lattice realization of the PR LP FBs. The organization of the paper is as follows. The properties of multirate filter banks are studied in Section II. The polyphase matrix and lattice factorization are discussed in Section III. Multiplier-less and SOPOT representation are discussed in Section IV. In Section V, design examples and discussions are presented. Finally, a conclusion is drawn in Section VI.

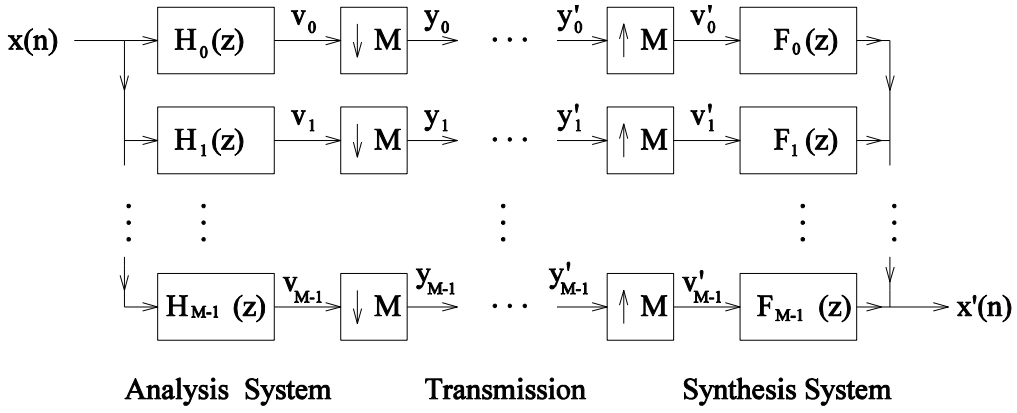


Fig. 1 Analysis and synthesis subsystems in a filter bank

## II. MUULTIRATE FILTER BANKS

a . Aliasing-free filter banks

Fig. 1 shows analysis/synthesis systems in a filter bank, where analysis and synthesis filters are denoted as $H_k(z)$, $0 \leq \quad \leq \quad -$ and $F_k(z)$, $0 \leq \quad \leq \quad -$, respectively. As shown in Fig. 1, a decimator is preceded by a band-limiting filter $H_k(z)$, $0 \leq \quad \leq \quad -$ whose purpose is to avoid the aliasing in Fig. 2. An interpolator, on the other hand, is followed by a band-limiting filter $F_k(z)$, $0 \leq \quad \leq \quad -$ with the purpose of reducing the imaging in Fig. 3. In practice, for a given set of analysis filters $H_k(z)$, the synthesis filte rs $F_k(z)$ are chosen so that the effects of imaging in the interpolators reduce or cancel the effects of aliasing caused by the decimators. The expression for the reconstructed signal $\hat{X}(z)$ is of the form

$$\hat{X}(z) = \frac{1}{M} \sum_{\ell} \qquad \ell \qquad \ell \qquad , , \tag{1.}$$

where $W =$ . The aliasing items are represented by $X(zW^{-\ell}, \sum_{i=} H_i(zW^{-\ell}, F_i(z)$,

$\ell$ . Aliasing is canceled if and only if the following set of relations hold:

(2.)

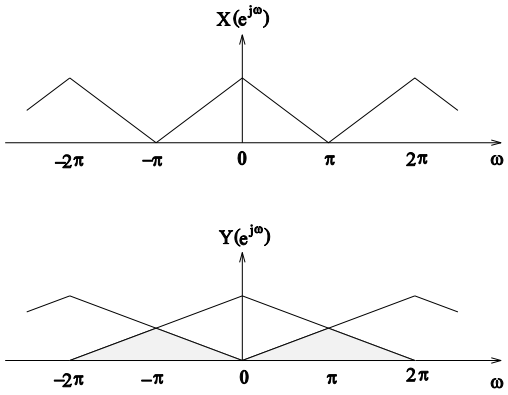


Fig. 2 The aliasing effects in a decimator

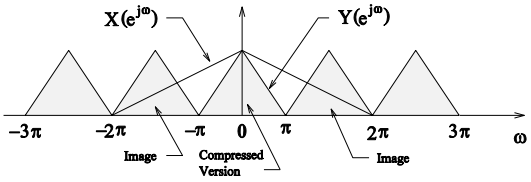


Fig. 3 The imaging effects in an interpolator

The above $M \times$ matrix on the left hand side has been referred to as the alias component matrix (AC matrix). Aliasing-free filter banks were first shown in the two-channel case in the quadrature mirror filters (QMF) and have found a number of applications in speech and image processing [14]. In $M$ -channel case, approximate cancellation of aliasing was shown and was accomplished with relatively complicated synthesis bank filters.

Once the aliasing has been canceled, the structure of Fig. 1 is time-invariant, and $\hat{X}(z)$ is related to $X(z)$ by a transfer function $T(z)$:

$$T(z) = \frac{\hat{X}(z)}{X(z)} = \frac{1}{M}\sum_{\ell} \quad \ell \qquad \ell \tag{3.}$$

The non-ideal amplitude and phase characteristic of $T(z)$ in (3) are the amplitude and phase distortions.

b. Perfect reconstruction filter banks

1) Definition

As shown above, there are several kinds of distortion sources in maximally decimated filter banks: aliasing/imaging, amplitude and phase distortions. In the past decades, much effort has been devoted to this area to achieve a perfect-reconstruction property. In a perfect-reconstruction filter bank, the overall transfer function in (3) is a pure delay,

$$T(z) = \tag{4.}$$

where $k$ is a constant and $r$ is an integer. The initial solutions allowing perfect reconstruction were addressed for the two-channel case. In the general case of an arbitrary number ($M$) of channels, a useful analysis tool is the polyphase representation.

2) Polyphase representation

Let the filters $H_i(z) = \sum_{n=-\infty}$ , $0 \le \ \le \ -$ be written as

$$H_i(z) = \sum_{l=} \tag{5.}$$

where $E_{i,l}(z)$ are the $z$-transforms of the $M$-fold decimated filters $e_{i,l}(n)$ defined by $e_{i,l}(n) = \ + \ , \ 0 \le \ \le \ - \ .$ Equation (5) is referred to as Type 1 polyphase representation and $E(z) =$ the polyphase matrix. The filters $H_i(z) = \sum_{n=-\infty}$ , $0 \le \ \le \ -$ can also be expressed as

$$H_i(z) = \sum_{l=} \qquad z^M), \tag{6.}$$

where $G_{i,l}(z) =$ $^{-\backslash}$. Equation (6) represents a variation of (5) by reversing the order of the polyphase components $E_{i,l}(z)$ and is defined as Type2 polyphase representation.

3) Implementation

With the polyphase representations in (5) and (6), the filter bank of Fig. 1 can be redrawn as in Fig. 4, where $E(z)$ and $R(z)$ are Type 1 and Type 2 polyphase matrices for the analysis filters $H_i(z)$, $0 \leq \ \leq \ -$ and synthesis filters $F_i(z)$, $0 \leq \ \leq \ -$, respectively. Using the standard identities, the subband filter bank in Fig. 4 can be further rearranged as in Fig. 5. A perfect reconstruction is obtained if the analysis and synthesis filters are chosen to satisfy the following property

$$R(z) = \qquad , \qquad \text{for all } z. \tag{7.}$$

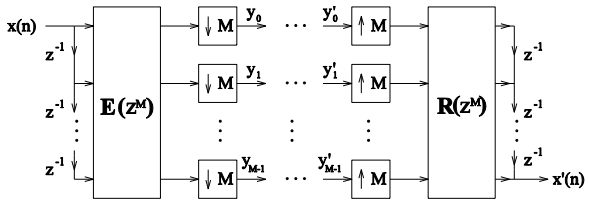


Fig. 4 Polyphase realization of maximally decimated filter banks

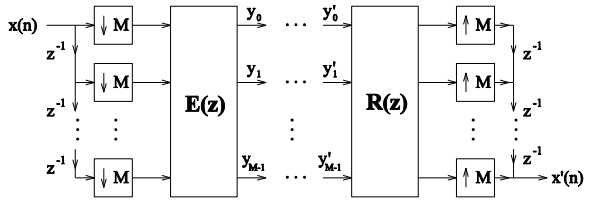


Fig. 5 An equivalent polyphase structure

## III. LATTICE FACTORIZATION

The unitary matrices in the lattice structures are implemented using a set of rotation matrices, which are then represented as sum-of-powers-of-two (SOPOT) coefficients using the approach. Let the analysis and synthesis filters be $H_k(z)$ , $0 \leq \quad \leq \quad -$ and $F_k(z)$ , $0 \leq \quad \leq \quad -$ , respectively. The linear-phase property of the FB implies that the polyphase matrix $\mathbf{E}(z)$ satisfy,

$$\mathbf{E}(z) = \quad \mathbf{DE} \quad \mathbf{J}_M , \tag{8.}$$

where $M$ is the number of channels, $N$ is a non-negative integer, $\mathbf{D}$ is a diagonal matrix with $d_{jj} = \pm$ , and $\mathbf{J}_M$ is the exchange matrix given by

$$\mathbf{J}_\ell = \begin{pmatrix} & & \\ & \iddots & \\ & & \end{pmatrix}_{\ell \ \ell} . \tag{9.}$$

The filters $H_k(z)$, $0 \leq \quad \leq \quad -$ , of the FBs are of length $(N +$ . For perfect reconstruction, the polyphase matrix $\mathbf{E}_N(z)$ can further be written as the following lattice structure

$$\mathbf{E}(z) = \mathbf{SPT} \quad \mathbf{P\Lambda}(z)\mathbf{PT}_{N-} \ \mathbf{P\Lambda}(z)\mathbf{P} \cdots \quad \mathbf{P} \tag{10.}$$

where

$$\mathbf{P} = \begin{pmatrix} \mathbf{I} & \mathbf{0} \\ \mathbf{0} & \mathbf{J} \end{pmatrix}, \quad \mathbf{S} = \quad \begin{pmatrix} \mathbf{I} & \mathbf{J} \\ \mathbf{I} & \mathbf{J} \end{pmatrix}, \quad \mathbf{\Lambda}(z) = \begin{pmatrix} \mathbf{I} & \\ & \mathbf{I} \end{pmatrix}, \tag{11.}$$

and

$$\mathbf{T}_i = \begin{pmatrix} \mathbf{A} & \mathbf{C} \\ \mathbf{C} & \mathbf{A} \end{pmatrix} \quad \begin{pmatrix} \mathbf{I} & \mathbf{I} \\ \mathbf{I} & \mathbf{I} \end{pmatrix} \begin{pmatrix} \mathbf{W} & \mathbf{0} \\ \mathbf{0} & \mathbf{U} \end{pmatrix} \begin{pmatrix} \mathbf{I} & \mathbf{I} \\ \mathbf{I} & \mathbf{I} \end{pmatrix}, \tag{12.}$$

where $\mathbf{W}_i$ and $\mathbf{U}_i$ are unitary matrices, and $\mathbf{I}_{M/2}$ is the (M/2)x(M/2) identity matrix.

## IV. MULTILPLIER-LESS AND SOPOT IMPLEMENTATION

The unitary matrices $\mathbf{W}_i$ and $\mathbf{U}_i$ in (12) can be factorized into a set of (2x2) rotation matrices in the following form

$$\mathbf{R}_{\theta} = \begin{pmatrix} & \\ & \end{pmatrix}. \tag{13.}$$

An example factorization of an ( $n \times$ ) orthogonal matrix is shown in Fig. 6, where $0 \leq \leq -$ , $i < \leq -$ . To achieve multiplier-less realization, this matrix $\mathbf{R}_{\theta}$ is first factored as follows

$$\mathbf{R}_{\theta} = \begin{pmatrix} & \\ & \end{pmatrix} \begin{pmatrix} & \\ & \end{pmatrix} \begin{pmatrix} & \\ & \end{pmatrix}, \tag{14.}$$

where $\alpha_{\_} =$ and $\beta_{\_} =$ . $\alpha_{\_}$ and $\beta_{\_}$ are then approximated by the following SOPOT coefficients

$$\alpha_{\_} = \sum_{k=}^{\cdot} \quad , \; a_k \in - \quad , \; b_k \in - _{\_} \quad - \quad _{2}\}, \tag{15.}$$

$$\beta_{\_} = \sum_{k=}^{\cdot} \quad , \; c_k \in - \quad , \; d_k \in - _{\_} \quad - \quad _{2}\}, \tag{16.}$$

where $- _{\_}$ and $r_2$ are the smallest and largest SOPOT coefficients, respectively. The number of terms being used in each coefficient is denoted as $t$, which is limited to a small number so that multiplication can be implemented with limited shifts and additions to achieve multiplier-less realization. The inverse of the rotation matrix is

$$\mathbf{R}_{\theta}^{-} = \begin{pmatrix} & \\ & \end{pmatrix} \begin{pmatrix} & \\ & \end{pmatrix} \begin{pmatrix} & \\ & \end{pmatrix}, \tag{17.}$$

which involves the same set of SOPOT coefficients. Therefore, the synthesis filter bank can also be built using a similar lattice structure with the same set of SOPOT coefficients $\alpha_{\_}$ and $\beta_{\_}$ .

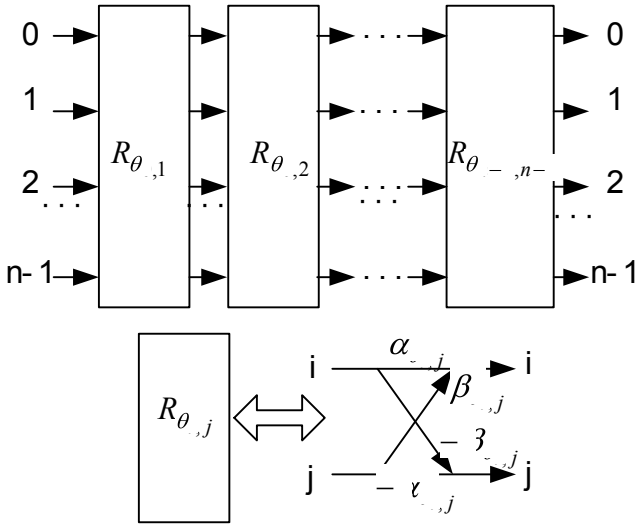


Fig. 6 Lattice factorization of an $(n \times$ orthogonal matrix.

## V. EXPERIMENTS AND DISCUSSIONS

a. Algorithms and experiments

In the experiments, the linear phase filter banks are designed with an iterative algorithm with five steps: (1) Initialization; (2) Lattice factorization; (3) Accumulation of pass-band and stop-band errors; (4) Conjugate gradient algorithm; (5) SOPOT multiplier-less approximation; The algorithm is summarized as follows.

1) Initialization: Select initial values for the frequency ranges of the analysis filters $H_k(z)$, $0 \leq \quad \leq \quad -$ in a filter bank in Fig. 1 as $[\omega_{\cdot\cdot} \ \omega_{\cdot\cdot}$, $[\omega_{\cdot} \ \omega_{\cdot}$, and $[\omega_{\cdot\cdot} \ \omega_{\cdot\cdot}$, where $p$, $t$ and $s$ stand for pass-band, transition-band, and stop-band, respectively. The subscription $r$ and $l$ denote the right and left limits of frequency range, respectively. Random numbers are also generated and shall be used to initialize the unitary matrices $\mathbf{W}_i$ and $\mathbf{U}_i$ in the lattice factorization as described in the following steps.

2) Lattice factorization: The polyphase matrix $\mathbf{E}(z)$ in (10) is formulated as the lattice factorization in (10)-(12), where the unitary matrices $\mathbf{W}_i$ and $\mathbf{U}_i$ in (12) are further factorized into a set of $(2 \times$ rotation matrices in (13).

3) Accumulation of pass-band and stop-band errors: The unitary property of the polyphase matrix $\mathbf{E}(z)$ and power complementary property in pass-bands and stop-bands among the channels are utilized to construct the objective function $\Omega$. The symmetry and anti-symmetry in linear phase filter banks can also be exploited in formulating the objective function. For filter banks with high orders $N$ in (8) and (10), fast Fourier transform (FFT) can be employed to reduce the computational complexity and finite precision effects caused by round-off errors.
4) Conjugate gradient algorithm: Conjugate gradient algorithm can be applied to optimize the planar rotations $\theta$ in (13)-(17). The frequency responses are optimized to meet the prescription of stopband attenuations.
5) SOPOT multiplier-less approximation: To facilitate multiplier-less approximation, the planar rotation matrix $\mathbf{R}_\theta$ in (13) is factorized as (14). In the SOPOT representation, $\alpha$ and $\beta$ are then approximated with (15) (16). In a filter bank with $M$ multiplicative elements ($\lambda$, $\lambda \cdots, \lambda$, the system response $T$ can be expressed as $T =$ $, \lambda, \cdots, \lambda$. Let [$\lambda$ denote the multiplier-less representation of $\lambda$ with $n_i$ adders. Let $\hat{T}$ be the multiplier-less approximation of $T$ and be expressed as $\hat{T} =$ $, [\lambda, \cdots, [\lambda$. The total number of adders can be written as $N_{\hat{T}} =$ $+\sum_{i=}^{}$. The term $N_0$ stands for the "inherent" number of adders in the filter bank, i.e., the residue number of adders even when all the multiplication coefficients ($\lambda$, $\lambda \cdots$, $\lambda$ are set to 1. For example, $N_0$ in $T = \times \times$ is 1, as one "inherent" adder is found in $T$. On the other hand, $N_0$ in $T = \times \times$ is 0, as no "inherent" adder is found in $T$. In the multiplier-less approximation algorithm, the total number of available adders is constrained, i.e., $N_{\hat{T}} \leq$. The multiplier-less approximation algorithm seeks to optimally distribute a total number ($N -$) of adders among all the multiplicative elements ($\lambda, \lambda \cdots, \lambda$ so that the deviation error of $\hat{T}$ from \$T\$ is minimized in a predefined criteria. In the experiment, we adopt the least-mean-square (LMS) error as the performance criteria. The sequential allocation algorithm (SAA) is employed in the experiment. It allocates one adder to the most

"effective" multiplier $\lambda$ in each round. The most "effective" multiplier is the one that would give the least approximation error among all the multiplier ($\lambda$ , $\lambda$ ⋯, $\lambda$ . The iterative process proceeds until all the available adders are exhausted.

b. Experimental results and discussions

Fig. 7 shows the magnitude responses of an 8-channel SOPOT filter bank obtained by the proposed method. It can be observed that all the filters have stop band attenuations over 20 dB. The impulse responses of the 8-channel SOPOT filter bank are shown in Table 1. The filters are of length {24, 24, 24, 24, 24, 24, 24 and 24}. Because of the linear-phase property, only the first 12 samples $h_k(0)$, $h_k(1)$, …, $h_k(11)$ are tabulated. The remaining 12 samples $h_k(12)$, $h_k(13)$, …, $h_k(23)$ can be determined by the symmetry/anti-symmetry of analysis filters. The filters in channel 0, 2, 4, 6 are symmetric while the filters in channel 1, 3, 5, 7 are anti-symmetric. The SOPOT coefficients $\alpha$ and $\beta$ for $\mathbf{W}_\theta$ and $\mathbf{U}_\theta$ in the lattice structures are displayed in Table 2 and Table 3, respectively. The subscript $m$ in $\theta$ is used to differentiate the independent planar rotations in $\mathbf{W}_i$ or $\mathbf{U}_i$. When the number ($M$) of channel is even, each sub-matrix $\mathbf{W}_i$ or $\mathbf{U}_i$ in (12) requires (($M$ / 2) × − independent planar rotations $\theta$ . As the number of $T_i$ in (10) is $N$ + , the number of $\mathbf{W}_i$ in (10) is $N$ + and the number of $\mathbf{U}_i$ in (10) is $N$ + . Hence, the total number of planar rotations is 2 × + × − , or ($N$ + − . Similarly, for the case when the number ($M$) of channel is odd, it can be shown that the total number of planar rotations is ($N$ + − + . In Fig. 7, the number ($M$) of channels in the filter bank is 8 and $N$ + is 3. By substituting $M$ and $N$ + to ($N$ + − , the total number of planar rotations $\theta$ is 18. It is consistent with the observation that there are 18 rows in Table 2 and Table 3. In the experiments, the conjugate gradient algorithm is employed to search optimal values of planar rotations $\theta$ in an 18 dimensional parameter space for the nonlinear function $\Omega$. For filter banks with a parameter space of high dimension to search, more than one set of initial values should be employed and the resulted filters are selected to avoid the problem of local minimum in designing the floating-point coefficients by the conjugate gradient algorithm.

Table 1: Impulse responses of 8-channel SOPOT filter banks

| $n$ | $h_0(n)$ | $h_1(n)$ | $h_2(n)$ | $h_3(n)$ |
|---|---|---|---|---|
| 0 | -0.005336 | 0.013032 | -0.011571 | -0.002494 |
| 1 | -0.005108 | 0.005148 | -0.004309 | -0.000623 |
| 2 | -0.006042 | 0.008393 | -0.003295 | 0.006699 |
| 3 | -0.015215 | 0.004426 | 0.001650 | 0.003358 |
| 4 | -0.021915 | 0.035720 | -0.017008 | 0.024019 |
| 5 | 0.009044 | 0.030617 | -0.048899 | -0.026869 |
| 6 | 0.018585 | 0.012751 | -0.046939 | -0.076080 |
| 7 | 0.043321 | -0.040332 | 0.035753 | 0.012693 |
| 8 | 0.093588 | -0.118828 | 0.119920 | 0.124015 |
| 9 | 0.112551 | -0.153744 | 0.116121 | 0.059580 |
| 10 | 0.132910 | -0.131523 | -0.015586 | -0.144894 |
| 11 | 0.140054 | -0.052020 | -0.166959 | -0.114357 |
| $n$ | $h_4(n)$ | $h_5(n)$ | $h_6(n)$ | $h_7(n)$ |
| 0 | 0.001050 | 0.005861 | 0.007994 | -0.002069 |
| 1 | -0.001498 | -0.005324 | -0.006040 | 0.004789 |
| 2 | -0.007094 | 0.000903 | 0.005996 | -0.003100 |
| 3 | 0.006228 | 0.001431 | -0.005509 | 0.015985 |
| 4 | -0.028193 | 0.004697 | 0.026283 | -0.015613 |
| 5 | -0.026063 | -0.051136 | -0.038538 | -0.008565 |
| 6 | 0.076924 | 0.046099 | 0.014699 | 0.009734 |
| 7 | -0.001581 | 0.035927 | 0.049773 | -0.047041 |
| 8 | -0.132892 | -0.140030 | -0.113126 | 0.080031 |
| 9 | 0.037724 | 0.114625 | 0.158983 | -0.110656 |
| 10 | 0.152508 | 0.020681 | -0.119958 | 0.127193 |
| 11 | -0.100508 | -0.139821 | 0.055651 | -0.148909 |

Table 2: SOPOT coefficients of $\alpha_{\_}$ and $\beta_{\_}$ in $\mathbf{W}_{\theta}$

| $\theta$ | $\alpha_{\_}$ | $\beta_{\_}$ |
|---|---|---|
| $\theta$ | $1-\quad+\quad-$ | $2^{-}-\quad+\quad-$ |
| $\theta$ | $1$ | $1$ |
| $\theta$ | $1$ | $1-\quad+$ |
| $\theta$ | $2^{-}$ | $2^{-}-$ |
| $\theta$ | $1-\quad+$ | $1-\quad+\quad-\quad+$ |
| $\theta$ | $1-\quad+\quad-\quad+$ | $2^{-}-$ |
| $\theta$ | $1-$ | $1-\quad+$ |
| $\theta$ | $1-\quad+\quad-$ | $2^{-}-\quad+$ |
| $\theta$ | $1-\quad+$ | $1-$ |
| $\theta$ | $1-\quad+$ | $1-\quad+\quad-\quad+$ |
| $\theta$ | $1$ | $1-\quad+$ |
| $\theta$ | $2^{-}$ | $2^{-}$ |
| $\theta$ | $1-$ | $1-\quad+$ |

| | | |
|---|---|---|
| $\theta_{\cdot\cdot}$ | $2^{-}-\quad+\quad-$ | $2^{-}-\quad+$ |
| $\theta_{\cdot\cdot}$ | $1-\quad+$ | $2^{-}-\quad+\quad-$ |
| $\theta_{\cdot\cdot}$ | $1-\quad+$ | $1-\quad+\quad-$ |
| $\theta_{\cdot\cdot}$ | $1$ | $1-$ |
| $\theta_{\cdot\cdot}$ | $1-\quad+\quad-$ | $2^{-}-\quad+$ |

Table 3: SOPOT coefficients of $\alpha_{\cdot}$ and $\beta_{\cdot}$ in $\mathbf{U}_{\theta}$

| $\theta_{\cdot}$ | $\alpha_{\cdot}$ | $\beta_{\cdot}$ |
|---|---|---|
| $\theta_{\cdot\cdot}$ | $1$ | $1-\quad+$ |
| $\theta_{\cdot\cdot}$ | $2^{-}$ | $0$ |
| $\theta_{\cdot\cdot}$ | $2^{-}-$ | $2^{-}-$ |
| $\theta_{\cdot\cdot}$ | $1-$ | $1-$ |
| $\theta_{\cdot\cdot}$ | $2^{-}-$ | $2^{-}$ |
| $\theta_{\cdot\cdot}$ | $2^{-}-\quad+$ | $2^{-}-\quad+$ |
| $\theta_{\cdot\cdot}$ | $1-\quad+\quad-$ | $2^{-}-\quad+$ |
| $\theta_{\cdot\cdot}$ | $1$ | $1$ |
| $\theta_{\cdot\cdot}$ | $1-\quad+$ | $1-\quad+\quad-\quad+$ |
| $\theta_{\cdot\cdot}$ | $1-$ | $1-\quad+$ |
| $\theta_{\cdot\cdot}$ | $1-\quad+$ | $2^{-}$ |
| $\theta_{\cdot\cdot}$ | $2^{-}-$ | $2^{-}$ |
| $\theta_{\cdot\cdot}$ | $1$ | $1-$ |
| $\theta_{\cdot\cdot}$ | $2^{-}$ | $2^{-}-$ |
| $\theta_{\cdot\cdot}$ | $1-$ | $1-\quad+\quad-$ |
| $\theta_{\cdot\cdot}$ | $2^{-}-\quad+\quad-$ | $2^{-}-\quad+$ |
| $\theta_{\cdot\cdot}$ | $1-\quad+$ | $2^{-}-\quad+\quad-$ |
| $\theta_{\cdot\cdot}$ | $1-\quad+$ | $1-\quad+\quad-$ |

After optimizing the floating-point values of planar rotations $\theta$ , the sequential allocation algorithm (SAA) is employed. The results of multiplier-less approximation are tabulated in Table 2 and Table 3. Among the 36 coefficients ($\alpha$ , $\beta$ ) in Table 2, 8 coefficients have only one term of $2^{-}$ , which indicates that no addition is needed in multiplier-less implementation. In Table 2, there are also 6, 11, 7, 4 coefficients with 2, 3, 4, 5 terms of $2^{-}$ , respectively. This implies 1, 2, 3 4 additions are required in multiplier-less implementation of each of these coefficients, respectively. It can be shown the total number of additions for the 36 coefficients, $\alpha$ and $\beta$ , is 56. The average number of additions for each of the 36 coefficients, $\alpha$ and $\beta$ , is 1.81. Among the 36 coefficients ($\alpha$ , $\beta$ ) in Table 3, one coefficient is 0, and 9 coefficients have only one term of $2^{-}$ . No addition is needed in multiplier-less implementation of these 10 coefficients. In Table 3, t there are 10, 10, 5, 1 coefficient have 2, 3, 4, 5 terms of $2^{-}$ , respectively. This implies 1, 2, 3 4 additions are required in multiplier-less implementation of each of these coefficients, respectively. It can be shown that the total number of additions for the 36 coefficients, $\alpha$ and $\beta$ , is 49. The average number of additions for each of he 36 coefficients, $\alpha$ and $\beta$ , is 1.36. In general, the approximation error will be reduced as the number of SOPOT terms ($t$ in (15) and (16)) increases. In the experiment, the maximum number of SOPOT terms in coefficients $\alpha$ and $\beta$ (Table 2 and Table 3) is $5$ and the filters are very close to the real-valued counterparts. Two 5-channel filter banks with a length distribution $(20, 20, 20, 20, 20)$ and $(30, 30, 30, 30, 30)$ are also shown in Fig. 8 and Fig. 9, respectively. In Fig. 8, the number $(M)$ of channels in the filter bank is 5 and $N$ is $3$. By substituting $M$ and $N$ to $(N +$ $-$ $+$ , the total number of planar rotations $\theta$ is $16$. In Fig. 9, the number $(M)$ of channels in the filter bank is $5$ and $N$ is $5$. By substituting $M$ and $N$ to $(N +$ $-$ $+$ , the total number of planar rotations $\theta$ is $24$. The conjugate gradient algorithm is employed to search optimal values of planar rotations $\theta$ in an 18 and 24-dimension space for the nonlinear function $\Omega$ for Fig. 8 and Fig. 9. As the coefficient multiplications can be implemented with limited number of additions, the implementation complexity of the filter banks is considerably reduced. Moreover,

filter banks are implemented with the lattice structures and the factorization in (14) and (17) and the perfect-reconstruction (PR) property is preserved, despite of the SOPOT approximation.

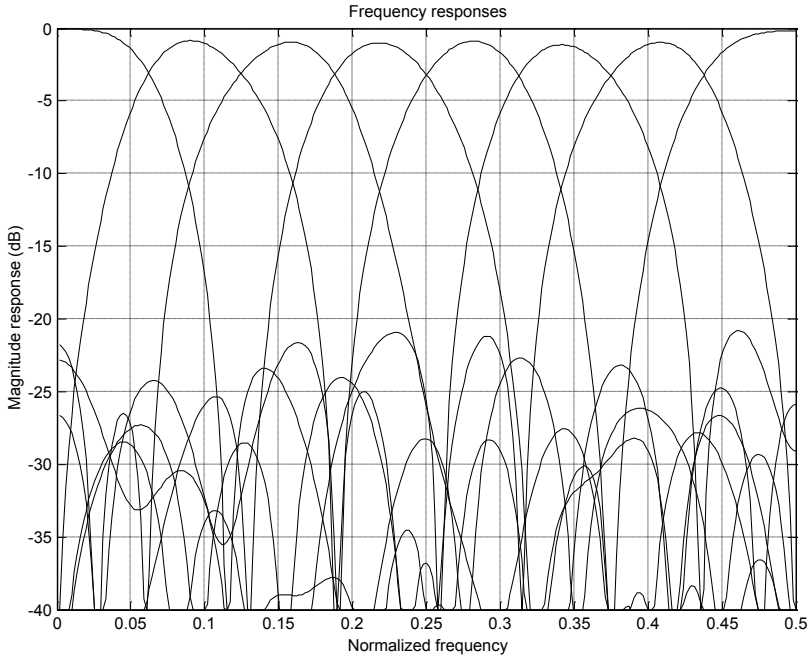


Fig. 7 Frequency responses of the proposed 8-channel SOPOT LP filter bank

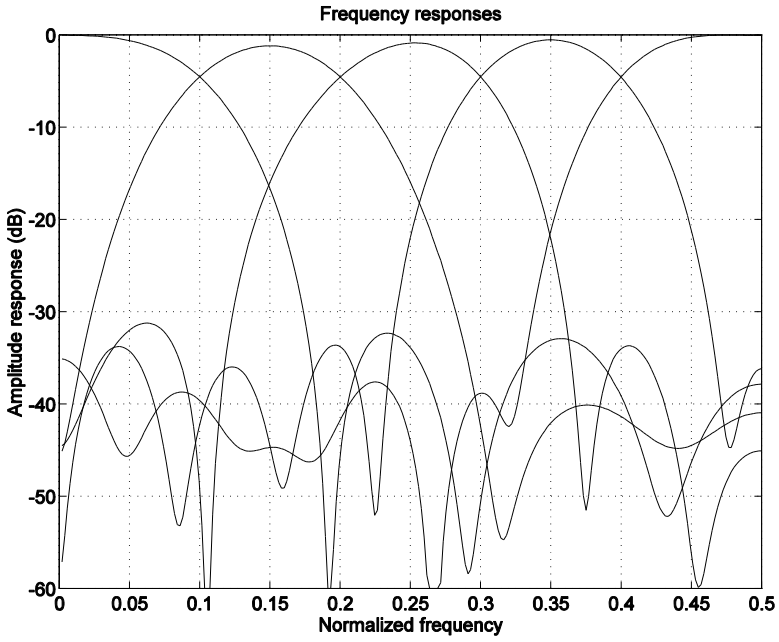


Fig. 8 A 5-channel filter bank with filter lengths (20, 20, 20, 20, 20)

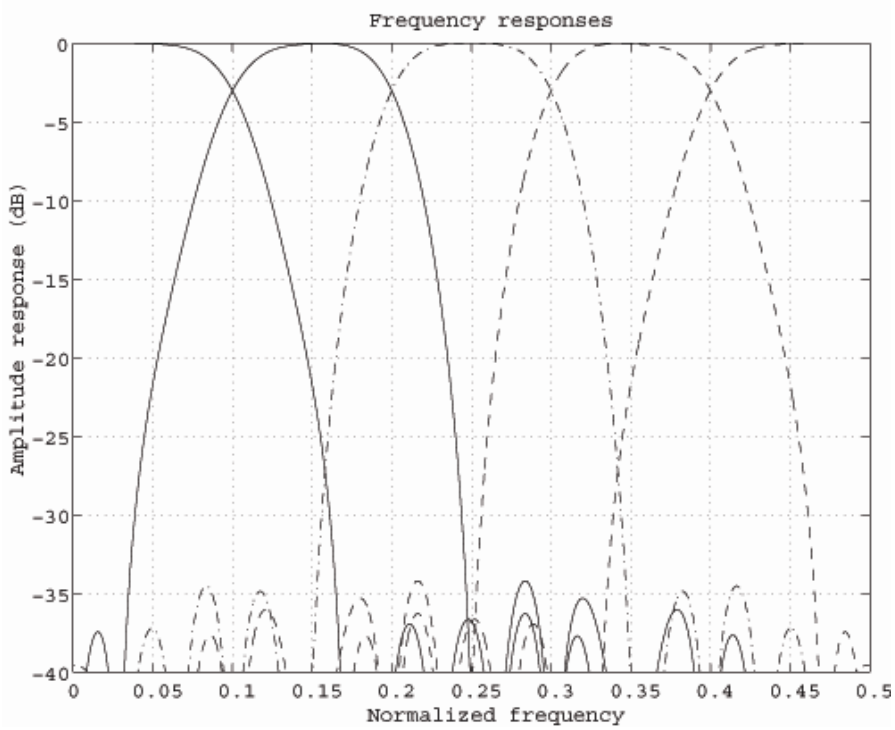


Fig. 9 A 5-channel filter bank (30, 30, 30, 30, 30)

## VI. CONCLUSIONS

A new multiplier-fewer algorithm for linear-phase perfection reconstruction filter banks has been presented by using multiplier-less approximation of the coefficients in the lattice structures. The property of perfection reconstruction is preserved, regardless the multiplier-less approximation of lattice structures in the factorization of polyphase matrix. Design examples of multiplier-less 5-channel and 8-channel linear-phase perfect reconstruction filter banks have been demonstrated. The coefficient multiplications have been replaced with a limited number of additions and hence the implementation complexity was significantly reduced. The multiplier-less linear-phase perfect reconstruction filter banks can be used in image data compression and signal enhancement.

## ACKNOWLEDGEMENTS

This work was supported in part by Natural Science Foundation of China (No. 60275011) and Guangdong Science Foundation (No. 021252).

## REFERENCES

[1] D. Taskovski and L. Koleva, "Measurement of harmonics in power systems using near perfect reconstruction filter banks," IEEE Trans. Power Delivery, vol. 27, no. 2, pp. 1025–1026, Apr. 2012.

[2] J. Barros and R. Diego, "Analysis of harmonics in power systems using wavelet packet transform," IEEE Trans. Instrumentation and Measurement, vol. 57, no. 1, pp. 63–69, Jan. 2008.

[3] C. Guan, P. B. Luh, L. D. Michel, Y. Wang, and P. B. Friedland, "Very short-term load forecasting: wavelet neural networks with data pre-filtering," IEEE Trans. Power Systems, vol. 28, no. 1, pp. 30–41, Feb. 2013.

[4] B. Lechner, M. Lieschnegg, O. Mariani, M. Pircher, and A. Fuchs, "A wavelet-based bridge weigh-in-motion system," International Journal of Smart Sensing and Intelligent Systems, vol. 3, no. 4, pp. 573–591, Dec. 2010.

[5] B. Huang, M. Yuan, G. Wu, X. Ling, and C. Wan, "Modeling to compiling: Design and implementation for wireless sensor network system," Journal of Theoretical and Applied Information Technology, vol. 48, no.1, pp. 113–119, Feb. 2013.

[6] F. J. Harris and M. Rice, "Multirate digital filters for symbol timing synchronization in software defined radios," IEEE Journal on Selected Areas in Communications, vol. 19, no. 12, pp. 2346–2357, Dec. 2011.

[7] D. D. Donno, F. Ricciato, and L. Tarricone, "Listening to Tags: Uplink RFID measurements with an open-source software-defined radio tool," IEEE Trans. Instrumentation and Measurement, vol. 62, no. 1, pp. 109--118, Jan. 2013.

[8] D. Xu and Y. Chen, "A safe RFID authentication protocol for internet of things," Journal of Theoretical and Applied Information Technology, vol. 48, no.1, pp. 215–220, Feb. 2013.

[9] X. Hao, W. Zhao and Y. Zhao, "Designation and simulation of equipment integrated PM2.5 and mercury removal," Journal of Theoretical and Applied Information Technology, vol. 48, no.1, pp. 442-447, Feb. 2013.

[10] V. Iyer, G. R. Murthy, and M. B. Srinivas,, "Training data compression algorithms and reliability in large wireless sensor networks," International Journal of Smart Sensing and Intelligent Systems, vol. 1, no. 4, pp. 912–921, Dec. 2012.

[11] A. Mahajan, C. Oesch, H. Padmanaban, L. Utterback, S. Chitikeshi, and F. Figueroa, "Physical and virtual intelligent sensors for integrated health management systems," International Journal of Smart Sensing and Intelligent Systems, vol. 5, no. 3, pp. 107–148, Mar. 2012.

[12] Y. Wei and D.-B. Liu, "A design of digital FIR filter banks with adjustable subband distribution for hearing aids", in Proc. 8th International Conference on Information, Communications and Signal Processing (ICICS), 2011, pp. 1-5.

[13] Y. Lian and Y. Wei, "A computationally efficient nonuniform FIR digital filter bank for hearing aids," IEEE Trans. Circuits and Systems I: Regular Paper, vol. 52, no. 12, pp. 2754–2762, Dec. 2005.

[14] J.-B. Maj, L. Royackers, M. Moonen, and J. Wouters, "SVD-based optimal filtering for noise reduction in dual microphone hearing aids: A real time implementation and perceptual evaluation," IEEE Trans. Biomedical Engineering, vol. 52, no. 9, pp. 1563–1573, Sept. 2005.

[15] Y. Deng, V. J. Mathews and B. Farhang-Boroujeny, "Low-delay nonuniform pseudo-QMF banks with application to speech enhancement", IEEE Trans. Signal Processing, vol. 55, no. 5, Part 2, pp. 2110–2121, May 2007.

[16] J. Sun and M. F. Tappen, "Separable Markov random field model and its applications in low level vision," IEEE Trans. Image Processing, vol. 22, no. 1, pp. 402–408, Jan. 2013.

[17] Q. Luo, L. Luo, Q. Ren, and H. He, "Optimization design of biorthogonal filter banks for image compressing," in Proc. International Symposium on Information Science and Engineering (ISISE), 2008, vol. 2, pp. 539 – 543.

[18] Q. Luo, L. Luo, Q. Ren, H. He, "Optimization design of biorthogonal filter bank for image compressing", in Proc. International Symposium on Information Science and Engineering, pp. 539-543, 2008.

[19] M. Riera-Guasp, M. Pineda-Sanchez, J. Perez-Cruz, R. Puche-Panadero, J. Roger-Folch and J. A. Antonino-Daviu, "Diagnosis of induction motor faults via Gabor analysis of the current in transient regime," IEEE Trans. Instrumentation and Measurement, vol.61, no.6, pp.1583-1596, June 2012.

[20] S. A. Saleh, "The implementation and performance evaluation of 3φ VS wavelet modulated AC-DC converters," IEEE Trans. Power Electronics., vol. 28, no. 3, pp. 1096--1106, Mar. 2013.

[21] O. Jahromi, Multirate Statistical Signal Processing, New York: Springer-Verlag, 2007.

[22] A. Fernandez-Vazquez and G. J. Dolecek, "Maximally flat CIC compensation filter: design and multiplierless implementation," IEEE Trans. Circuits and Systems II: Express Briefs, vol. 59, no. 2, pp. 113-117, Feb. 2012.

[23] B. Y. Kong and I.-C. Park, "FIR filter synthesis based on interleaved processing of coefficient generation and multiplier-block synthesis," IEEE Trans. Computer-Aided Design of Integrated Circuits and Systems, vol.31, no.8, pp. 1169-1179, Aug. 2012.

[24] N . H . Cuong, N. T. Lam, and N. D. Minh, "Multiplier-less based architecture for variable-length FFT hardware implementation," in Proc. Fourth International Conference on Communications and Electronics (ICCE), pp. 489-494, Aug. 1-3, 2012.

[25] M. B. Gately, M. B. Yeary, C. Y. Tang, "Multiple real-constant multiplication with improved cost model and greedy and optimal searches," in Proc. IEEE International Symposium on Circuits and Systems (ISCAS), pp.588-591, May 20-23, 2012.

[26] M. Joliveau, P. Giard, M. Gendreau, F. Gagnon and C. Thibeault, "Design of low complexity multiplierless digital filters with optimized free structure using a population-based metaheuristic," in Proc. 10th International Symposium on Signals, Circuits and Systems (ISSCS), pp.1-4, Jun. 30 -Jul. 1, 2011.

[27] G. S. Baicher, "Towards optimal implementation of a class of quadrature mirror filter using genetic algorithms", in Proc. IEEE Fifth International Conference on Bio-Inspired Computing: Theories and Applications (BIC-TA), pp. 1663-1668, 2010.

[28] P. S. R. Diniz, L. C. R. de Barcellos and S. L. Netto, "Design of high-resolution cosine-modulated transmultiplexers with sharp transition band," IEEE Trans. Signal Processing, vol. 52, no. 5, pp. 1278–1288, May 2004.

[29] X.-D. Xu, "Design of cosine-modulated filter banks with large number of channels based on FRM technique," in Proc. International Conference on Computer Science and Network Technology, Dec. 24-26, 2011, pp. 776–780.

[30] M. Laddomada, D. E. Troncoso and G. J. Dolecek, "Design of multiplierless decimation filters using an extended search of cyclotomic polynomials," IEEE Trans. Circuits and Systems II: Express Briefs, vol. 58, no. 2, pp. 115-119, Feb. 2011.